Oxidation of CH4 by CO2 in a dielectric barrier discharge

Oxidation of CH_4 by CO_2 in a dielectric barrier discharge

L.M. Martini[a], G. Dilecce[a c d], G. Guella[a], A. Maranzana[b], G. Tonachini[b], P. Tosi[a*]

[a] *Dipartimento di Fisica, Università di Trento, Via Sommarive 14, I-38123 Povo, Italy*

[b] *Dipartimento di Chimica, Università di Torino, Corso Massimo D'Azeglio 48, I-10125, Torino, Italy*

[c] *Istituto di metodologie inorganiche e dei plasmi - CNR - UOS di Bari, via Orabona, 4 - 70125 Bari, Italy*

[d] *Istituto dei materiali per l'elettronica e il magnetismo - CNR - UOS di Trento, via alla cascata 56 c, I-38123 Povo, Italy*

** Corresponding author. +39 0461 281557 email: paolo.tosi@unitn.it*

Abstract

In the plasma dry reforming, CH_4 and CO_2 are dissociated by electron collisions producing fragments that in turn react to form new molecules. While the production of CO, H_2, and small hydrocarbons has been investigated extensively, much less is known about the plasma synthesis of oxygenated molecules, which is the target of the present work. In addition to experimental results, gas phase reactions for the production of acetic, formic and propanoic acid were investigated by DFT calculations.

keywords: dry reforming; dielectric barrier discharge; CH_4 oxidation; CO_2; TST

1. Introduction

The conversion of CH_4 and CO_2 to useful chemicals, although not a feasible route for an effective reduction of greenhouse gases in the atmosphere, is a central topic in current research on renewable and sustainable energy [1]. Beyond established methods, non thermal plasmas (NTP) have been explored for their capability to create, at low temperature, highly reactive species, which can activate very stable molecules as methane and carbon dioxide. Depending on the particular experimental set-up and the specific operational features, different chemicals are produced into the discharge in addition to the most abundant products CO and H_2: gaseous hydrocarbons [2,3,4] liquid hydrocarbons [5] and oxygenates [6,7]. Despite some significant efforts [8,9], little is known so far about both the reaction mechanisms and the possibility of controlling the product selectivity. Progress was recently made in understanding the synergistic effect of NTP and heterogeneous catalysis: although the use of plasma in combination with solid catalysts has shown to enhance the conversion efficiency [10], in the present work we have chosen to avoid the use of catalysts, trying to get some insights on the pure plasma-synthesis of oxygenates. Therefore, the purpose of this study is to contribute to a better understanding of the fundamental processes involved, rather than aiming to the achievement of better yield. We show that a partial control of the product selectivity can be achieved by modulating the electrical power delivered to the discharge, via a variable duty-cycle square wave (the duty cycle is defined as (Ton/T)x100, see figure 2). In such a way, we could control the residence time of the reactants into the discharge of a plug-flow reactor without changing the gas flux. By starting with the same molar amount of CO_2 and CH_4, the main oxygenates observed (listed according to their relative abundance) are methanol CH_3OH, acetic acid CH_3COOH, formic acid HCOOH, ethanol CH_3CH_2OH, propanoic acid CH_3CH_2COOH, and butanoic acid $CH_3(CH_2)_2COOH$. Higher yields of the heavier acids

(propanoic and butanoic) are obtained when the duration of the discharge phase is increased, which suggests a possible way to control the product selectivity. To offer an interpretation of the experimental findings, the reactions have been followed by investigating the stable structures that correspond to energy minima, and the transition structures (TS) which connect them.

2. Experimental

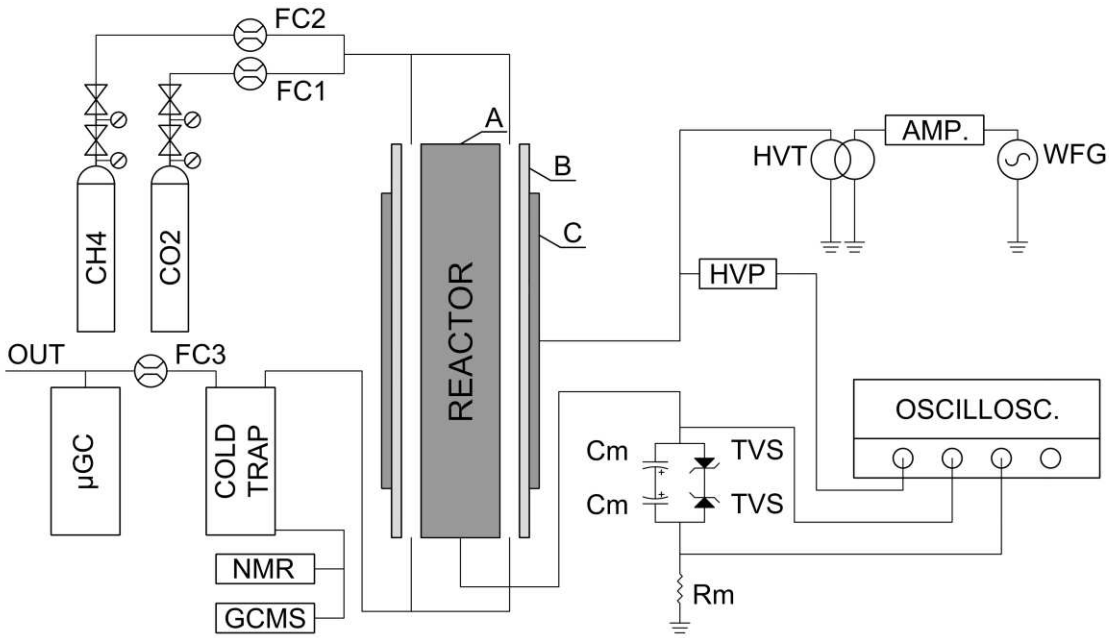

Figure 1: Schematic representation of the experimental set-up. WFG waveform generator; HVT high voltage transformer; HVP high voltage probe; C_m and R_m measurement capacitors and resistors, respectively; TVS transient suppressor voltage diode; FC1, FC2 mass flow controller; FC3 mass flow meter.

Figure 1 shows a diagram of the plasma reactor. The feed gases CH_4 and CO_2 (mixing ratio =1) was treated in a DBD reactor working at atmospheric pressure. It consists of a quartz tube (B, internal diameter 10 mm, external diameter 13 mm), externally coated with silver paint that acts as high voltage electrode (C), containing a concentric stainless steel cylinder (A, outer diameter 8 mm) that acts as grounded electrode. The reactor length is 170 mm. The gas mixture flows in the annular gap between the outer quartz tube (B) and the grounded electrode (A). CH_4 and CO_2 flow rates are both fixed at 0.1 SLM by mass

flow controllers FC1 and FC2, which implies a flow time between the electrodes of about 1.4 s. A trap cooled at approximately -18°C by ice and salted water is placed downstream the reactor to collect liquid products. Volatile products were analyzed by sampling the exhausts downstream the trap by a micro Gas Chromatograph mGC (Agilent 3000). Liquid compounds condensed into the cold trap were diluted in C_3D_6O or D_2O and quantitatively analyzed both by Gas Chromatography Mass Spectrometry GC-MS (Thermo-Finningan Trace GC - DSQ, DB-WAX Agilent J&W GC columns) and NMR (Avance 400 Bruker).

The DBD power supply is composed of a low voltage waveform generator (WFG, Agilent 33220A) coupled to a bridged class-D audio amplifier (Hypex UCD2k OEM). The amplifier is connected to a step-up high voltage transformer (Amp-Line Al-T1000.7-P100) operating in the range from 6 kHz to 11 kHz. The sinusoidal voltage at 8 kHz is modulated by a square wave of variable duty cycle and period t=1.12 s, see figure 2. The voltage applied to the electrodes is 17.5 kV_{pp} and is monitored by a high voltage AC probe (Tektronix P6015A). The internal electrode is connected to ground via a measurement circuit, made by an anti-series of tantalum capacitors C_m (1 μF) connected in parallel with an anti-series of zener unidirectional diodes, which act as overvoltage protection. The parallel is then connected in series with a 10 Ω resistor, R_m. Electrical signals are digitalized by a four channels oscilloscope (Agilent Infiniium 54831B) and used to estimate the power delivered to the discharge.

The electrical power is estimated by the Falkenstein-Coogan reformulation of the Manley's equation [11,12]. The power value was 47 ± 6 W (duty cycle 100%). As it is shown in figure 3, the discharge phase, occurring each half cycle, consists of several spatially separated discharge filaments. As a consequence only the fraction of the gas flow that is located into the filament is treated by the plasma. By changing the duty cycle we basically

vary the total number of micro discharges and therefore the specific energy deposition in the system.

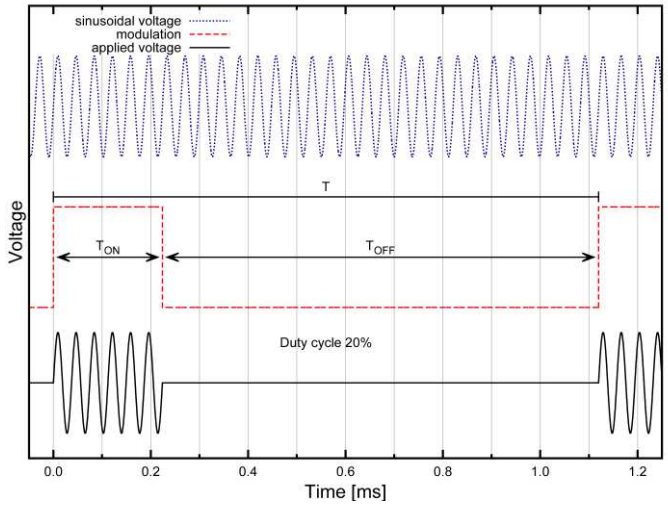

Figure 2: Modulation of the applied voltage by a square wave. The duty cycle is defined as $(T_{on}/T)x100$

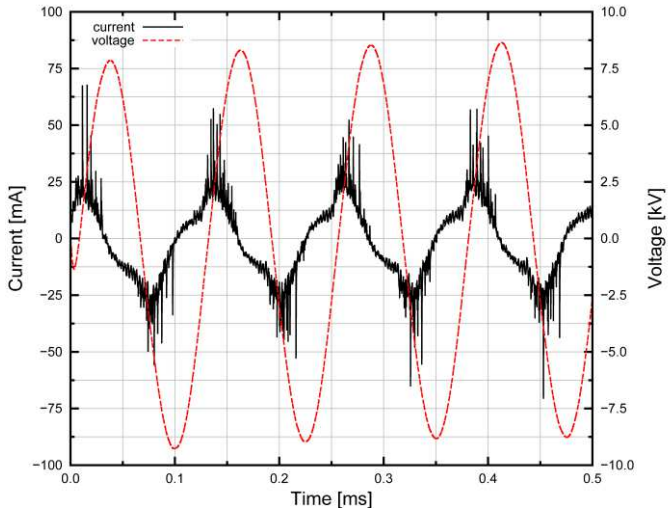

Figure 3: Plot of current and voltage versus time in our DBD

3. Computational methods

The attempt to offer an interpretation of the experimental results was conducted by carrying out quantum mechanical calculations, within the Density Functional Theory,[13] with the functional M06-2X.[14,15,16,17] Dunning's cc-pV*TZ* basis set was used.[18] The energy hypersurface was explored by gradient procedures.[19,20,21,22,23] This computational level, conventionally labelled as DFT(M06-2X)/cc-pV*TZ*, has been adopted for geometry optimizations and the subsequent vibrational analyses and thermochemistry assessments. For structures with diradicaloid character (two unpaired electrons in quasi-degenerate orbitals), the singlet energies were corrected for spin contamination by the triplet, by using a formula suggested by Yamaguchi.[24,25] The (corrected, if necessary) energies *E* were used in conjunction with the vibrational analysis data to evaluate the activation Gibbs free energies ($\Delta G^{\ddagger}$ at 400K), and zero-point vibrational energies (E_{ZPE}) [26]. When a first order saddle point, corresponding to a transition structure (TS), was present on the energy hypersurface, rate constants were estimated by using the Eyring equation within the Transition State Theory approximation [27]. When no TS on the energy hypersurface could be found (radical coupling) only an all-downhill path to the intermediate product was present. The *G* surface was then probed, looking for a possible maximum, by drawing *G* profiles along a path defined by series of constrained optimizations on the *E* surface, at fixed values of the distance R between the two moieties. Then, a vibrational analysis was performed by projecting out the vibrational frequency corresponding to the reaction coordinate [28]. ΔE_{ZPE} energy differences with respect to the reactants are reported in figures 6-8, while some computed *G* barriers are reported in the text, on the basis of which a rough estimate of the order of magnitude of the kinetic constants can be attempted (all energetics in $kJ \cdot mol^{-1}$ throughout the paper). All calculations were carried out by using the GAUSSIAN 09 program [29].

Geometrical parameters and total energies of reactants, products and transition structures are reported in the Supplementary Material.

4. Results and discussion

The percentage composition of the gaseous products detected on-line by the mGC indicates CO (48%) and H_2 (41%) as the more abundant species, followed by C_2H_6 (8.5%), C_3H_8 (1.5%) and traces (<1%) of C_2H_2 and C_2H_4. This trend appears to be in general agreement with values reported in literature [7, 30]. The percentage of the gaseous products does not change with the duty cycle, while the total yield increases. The CH_4 and CO_2 conversions vary linearly from about 2% at duty cycle 20 up to 12% and 6%, respectively, at duty cycle 100.

The mass balance indicates that, in addition to light gaseous species, about 2% (by weight) of the products condense into the cold trap, and are subsequently analyzed by GC-MS and NMR analysis. Results are shown in figures 4 and 5 as a function of the duty cycle of the discharge. Several oxidized products are formed into the discharge. NMR analysis carried out in D_2O (residual signal at δ_H = 4.82 ppm) shows the presence of methanol (δ_H = 3.43 ppm, singlet), ethanol (δ_H = 3.73 ppm, quartet; δ_H = 1.26 ppm, triplet), formic, (δ_H = 8.34 ppm, singlet), acetic (δ_H = 2.17 ppm, singlet), propanoic (δ_H = 2.47 ppm, quartet; δ_H = 1.17 ppm, triplet) and butanoic acid (δ_H = 2.42 triplet; δ_H = 1.67 ppm, sextet; δ_H = 0.98 ppm, triplet). Moreover, a strong singlet signal at δ_H = 4.90 ppm can be attributed to –O-CH_2-O- repeating unit of polyoxymethylene glycols. The origin of the latter relies on the plasma production of formic aldehyde which promptly reacts with water/methanol (in gas and/or liquid phase) leading to a complex mixture of polyoxymethylene glycols such as RO(-CH_2-O)$_n$-OR' (R,R' = H and/or CH_3).

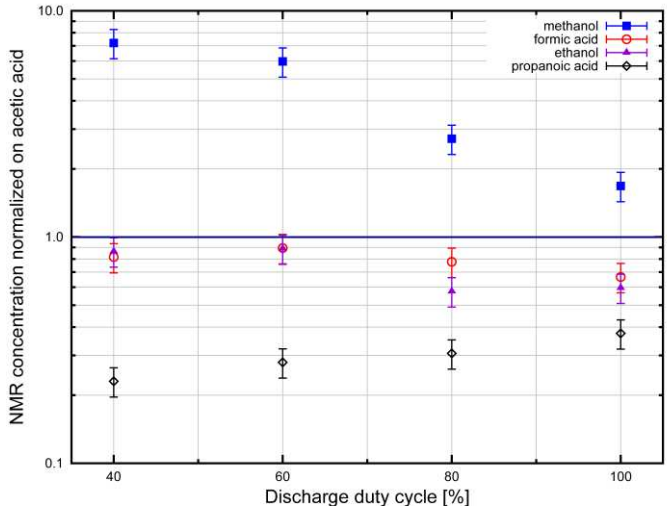

Figure 4: Relative concentration of different oxygenates (normalized on that of acetic acid, whose concentration is assumed to be equal to 1) as a function of the discharge duty cycle, as measured by NMR

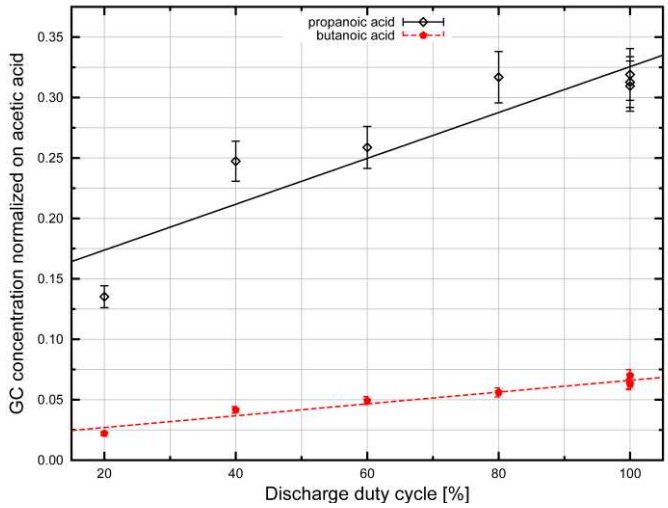

Figure 5: Concentration of different acids (normalized on that of acetic acid) as a function of the discharge duty cycle as measured by GC-MS

It is clear that by increasing the duty cycle of the discharge, i.e. the extent of the sinusoidal excitation, relative concentrations (normalized on that of acetic acid) of C_3 and C_4 compounds increase, while those of C_1 and C_2 compounds decrease. This result is in line with previous observations that at a constant discharge power, a low feed flow rate leads to produce higher hydrocarbons [10]. It is worth noting that while the selectivity depends on the product branching ratio, we have evidence that both terms of the ratio increase with the duty cycle. Thus the selectivity trend we are here discussing is not simply due to a decrease of acetic acid production. All together these findings support the idea that the

product selectivity can be switched from simple to more complex molecules by controlling the exposure of the species to the discharge phase, and thus the energy deposited in the system. To rationalize experimental findings, we have theoretically investigated the gas-phase formation of acetic, formic and propanoic acid, in particular estimating the relevant kinetic constants. For some of them a comparison of our results with experimental data is possible, for others these are not available. Electron impact processes on CH_4 and CO_2 mainly produce CH_3, H, CO and O. These species initiate a complex kinetic chain eventually resulting in the observed products. Hereafter we suggest possible pathways to the formation of acids.

4.1 Acetic acid formation

Three mechanisms could in principle lead to the acetic acid. They are shown in figure 6. The first one is the addition of carbon monoxide to a methyl radical, as it was already proposed [31]. The process (figure 6a) is characterized by a small barrier ($\Delta E^{\ddagger}_{ZPE}$ = 23.8 kJ mol^{-1}) and leads to the acetyl radical. A barrierless OH addition on the acetyl radical forms the acetic acid. The reaction between CH_3 and CO is well known in literature. Theoretical [32] and experimental [33] studies reported the rate coefficients for a large range of temperatures. At 400K the experimental rate is about 1.5×10^{-16} $molec^{-1}$ s^{-1} cm^3 [34], which is in satisfactory agreement with our theoretical value 5.2×10^{-15} $molec^{-1}$ s^{-1} cm^3 (calculated at the same temperature), once the accuracy attainable at our computational level is accounted for. It has to be stressed that the aim of this study is not to give quantitative estimates or reproduce accurately experimental rate constants, for which more accurate theoretical methods are mandatory, but to understand the possible pathways leading to the acids.

The acid could form also by a hydrogen abstraction from CH_4, operated by acetoxyl, or by a barrierless addition of H to acetoxyl CH_3CO_2 (figure 6b). However, acetoxyl radical is not

stable with respect to the reactants CH_3 + CO_2, with a high formation barrier (80.3 kJ mol^{-1}).

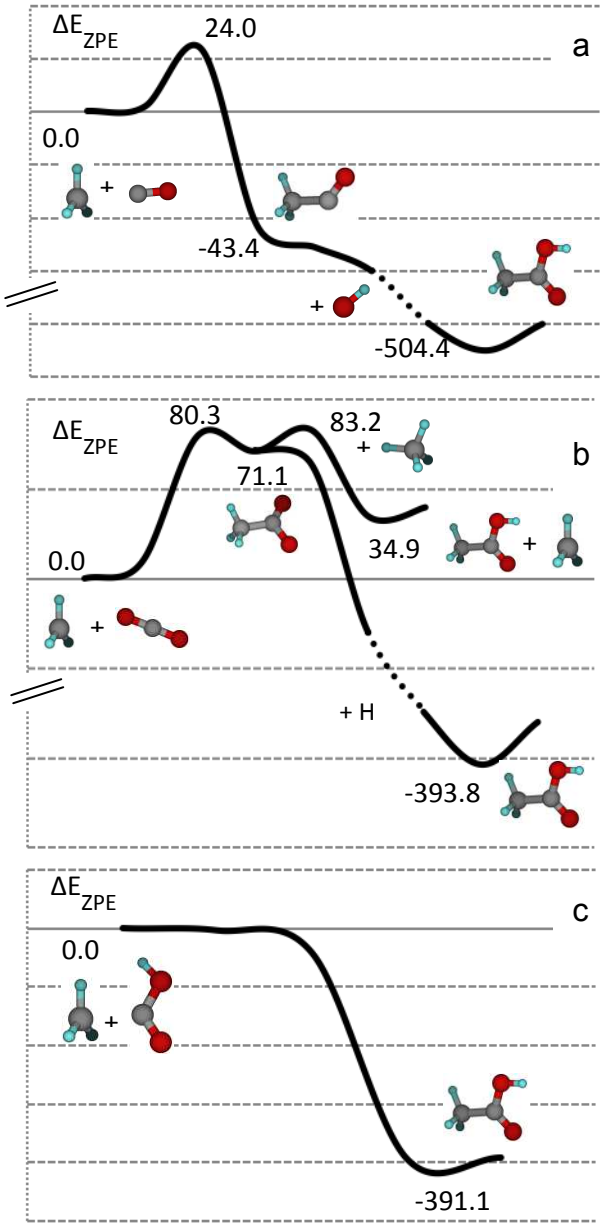

Figure 6. Acetic acid formation mechanisms: (a) methyl radical + CO, followed by HO addition; (b) methyl radical + CO_2, followed by H abstraction from CH_4, or H addition; (c) Methyl radical + HO-C=O radical. ΔE_{ZPE} energy differences in kJ mol^{-1}, with respect to the reactants.

A further pathway leading to acetic acid is the coupling reaction between methyl and carboxyl radicals (figure 6c), which occurs without any barrier on the potential energy

surface. To the best of our knowledge, no rate constant estimation is available for this reaction. The rate constant estimation is laborious, since no maximum along the energy profile is present, and a maximum can be found only along the approximate free energy profile itself. A series of constrained optimizations on the COOH + CH_3 system was carried out, in which the energy was minimized in correspondence of fixed values of the inter-carbon distance R between the two moieties. At each point the energy was corrected for spin contamination (see Method section). *G* was estimated by projecting out the imaginary frequency related to the relative motion along R. The *G* profile so obtained has a maximum for the rather large value R = 4.8 Å. The best estimate of the free energy barrier height results to be 23.8 kJ mol^{-1} (with respect to the reactants), and the corresponding rate constant is consequently roughly estimated of the order of 10^{-10} $molec^{-1}$ s^{-1} cm^3.

4.2 Propanoic and formic acid formation

The mechanisms for propanoic acid formation in figure 7 are similar to those described above for acetic acid. The barriers for intermediate and product formations and their stabilities are similar to those shown for acetic acid: the differences are within 10 kJ mol^{-1}.

CO addition to the ethyl radical (figure 7a) has been experimentally studied [35,36] and the reported rate constant at 400 K is 5.9×10^{-16} $molec^{-1}$ cm^3 s^{-1} [36], which is in good agreement with our theoretical estimate of 3.0×10^{-16} $molec^{-1}$ cm^3 s^{-1}. The addition of CO_2 is clearly unfavourable, as can be seen in figure 7b.

The C_2H_5 + COOH (figure 7c) rate constant was estimated as described in the preceding paragraph. The maximum on the free energy surface was found at R = 4.8 Å. The free energy barrier, with respect to C_2H_5 and COOH, is 28.2 kJ mol^{-1} and the rate constant is therefore roughly estimated of the order of 10^{-10} $molec^{-1}$ cm^3 s^{-1}.

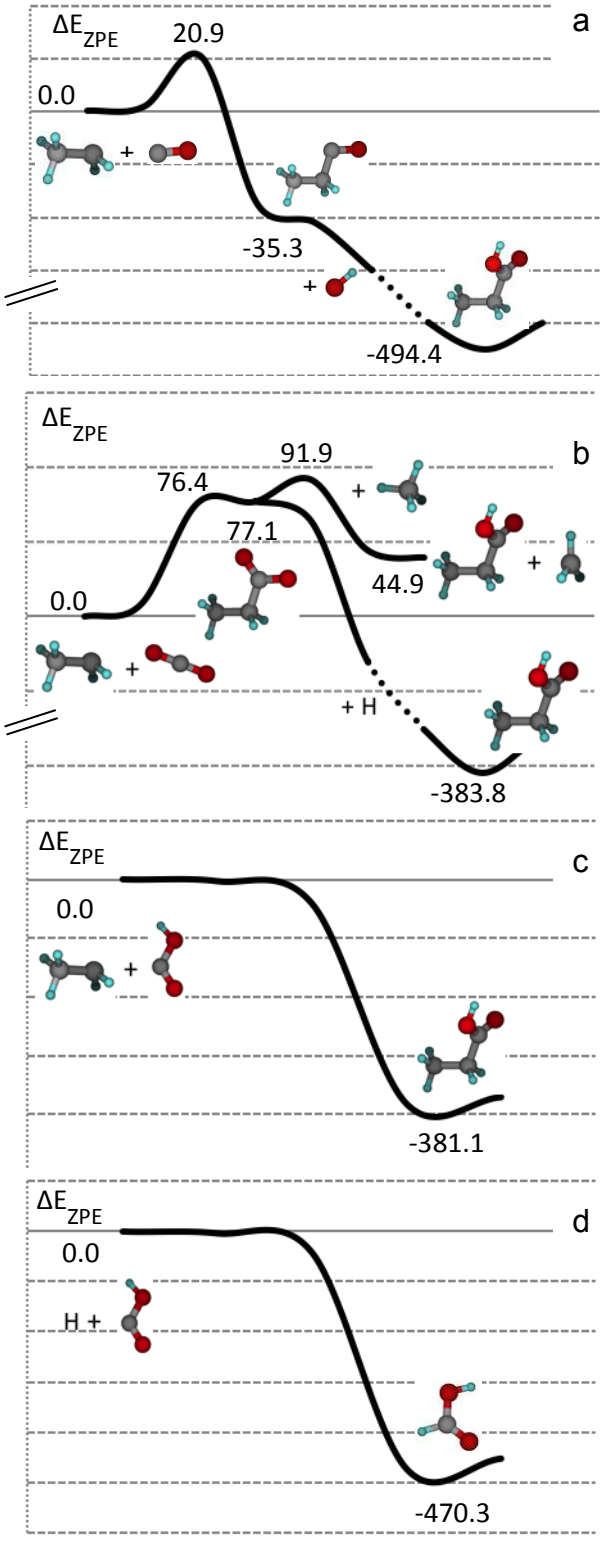

Figure 7. Propanoic and formic acid formation mechanisms: (a) ethyl radical + CO, followed by HO addition; (b) ethyl radical + CO_2, followed by H abstraction from CH_4, or H addition; (c) ethyl radical + HO-C=O radical; (d) H + HO-C=O radical coupling. ΔE_{ZPE} energy differences in kJ mol^{-1}, with respect to the reactants.

Formic acid (figure 7d) could be obtained by radical coupling between H and carboxyl radicals. In this case, the free energy barrier is 23.4 kJ mol^{-1} (R = 3.7 Å), and the rate is is roughly estimated at 400 K of the order of 10^{-10} $molec^{-1}$ cm^3 s^{-1}.

4.3 Carboxyl radical formation

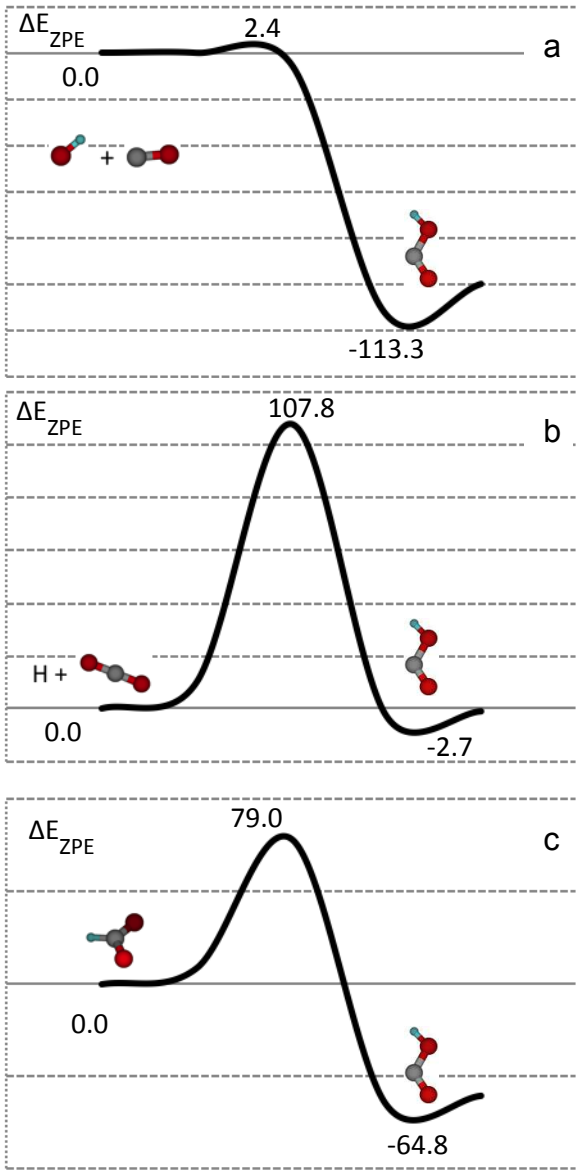

Figure 8. COOH radical formation: (a) HO radical + CO; (b) H + CO_2; (c) COOH isomerization. ΔE_{ZPE} energy differences in kJ mol^{-1}, with respect to the reactants.

The COOH radical seems to play a role on the acid formations, so it is important to understand how it could form. Of the three mechanisms shown in figure 8, the first one, CO + OH addition, shows the minimum barrier, 2.4 kJ mol^{-1} only, much lower than the barriers for the other two processes: H addition to CO_2 requires overcoming a barrier of ca. 108 kJ mol^{-1}, whereas the barrier for the isomerisation formyl radical - carboxyl radical is ca. 79 kJ mol^{-1}.

The CO + OH reaction has been theoretically extensively studied [37,38,39,40,41,42]. Our estimation for the carboxyl radical rate constant (at 400 K) is 1.5×10^{-12} $molec^{-1}$ cm^3 s^{-1}, very similar to the rate coefficient at high pressure limit reported by Klippenstein et al. (1.2×10^{-12} $molec^{-1}$ cm^3 s^{-1}) [41]. Our barrier (2.4 kJ mol^{-1}) comes out to be identical to that computed at CCSD(T)/cc-pV*TZ* by Yu et al. [42].

Reporting the reaction rates is not sufficient to identify the dominant mechanism for the formation of any of the oxygenates. As an example, by assuming a second order rate law, the rate of reaction for a radical-radical process becomes comparable with that of a radical-molecule process if the ratio between their rate constants is inversely proportional to the ratio between the respective densities. Consider reactions c and b in figure 6: an estimate of the ratio k_c/k_b gives 10^{12} and therefore their respective contributions to the production of acetic acid are comparable if the $[COOH]/[CO_2]$ ratio is around 10^{-12}. Thus to resolve this issue it is necessary to know the radical concentrations. While progress is being made, mainly based on optical spectroscopy techniques [43], some hints come from a recent computational study [30] where the ratio between overall radical and molecular densities is estimated to be $\approx10^{-4}$. As a consequence, the rate of reaction in figure 6c becomes comparable with that of reaction in figure 6b if the concentration of COOH is 10^{-8} that of the radicals. This specific example suggests that reactions between radicals may still play a role, even with very small reactant concentrations.

No matter what reactions give the main contributions, since acetic and propanoic acids are formed from CH_3 and C_2H_5 respectively (see reactions in figures 6 and 7), the ratio of propanoic to acetic acid is function of the ratio of C_2H_5 to CH_3. However C_2H_5 is produced starting from CH_3 + CH_3 and thus depends on $[CH_3]^2$. Eventually the ratio $[CH_3CH_2COOH]/[CH_3COOH]$ is a function of $[CH_3]$. This fact qualitatively explains the increase of CH_3CH_2COOH with respect to CH_3COOH as a function of the discharge duty cycle, as increasing the duty cycle involves the increase of $[CH_3]$ due to electron dissociation of CH_4.

Conclusions

In recent years, the interest in the process of dry reforming by plasma techniques has grown. While the production of syngas (H_2 and CO) is relatively well understood, much less is known about the synthesis of oxygenates. In the present work we report on the formation of various acids in a DBD of CH_4 and CO_2 at atmospheric pressure. The branching ratio of the oxygenates changes depending on the duty cycle of the discharge: it is observed that by increasing the duty cycle the ratio of propanoic-butanoic acids to acetic acid increases. In order to rationalize the experimental results, we have theoretically investigated possible mechanisms for the synthesis of acetic, formic and propanoic acids, suggesting some significant reactions and their rate constants. The selectivity of oxygenated products can be qualitatively explained by the dependence of the CH_3 production on the energy deposited in the system, via variation of the discharge duty cycle.

Acknowledgements

This work was partially supported by Provincia Autonoma di Trento and Istituto MCB of CNR (ENAM project)

References

[1] W. Wang, S. Wang, X. Ma, J. Gong, Recent advances in catalytic hydrogenation of carbon dioxide, Chem. Soc. Rev. 40 (2011) 3703–3727.

[2] S. Paulussen, B. Verheyde, X. Tu, C. De Bie, T. Martens, D. Petrovic, A. Bogaerts, B. Sels, Conversion of carbon dioxide to value-added chemicals in atmospheric pressure dielectric barrier discharges, Plasma Sources Sci. Technol. 19 (2010) 034015.

[3] I. Istadi, N.A.S. Amin, Co-generation of synthesis gas and C_{2+} hydrocarbons from methane and carbon dioxide in a hybrid catalytic-plasma reactor: A review, Fuel 85 (2006) 577–592.

[4] C.J. Liu, B.Z. Xue, B. Eliasson, F. He, Y. Li, G.H. Xu, Methane conversion to higher hydrocarbons in the presence of carbon dioxide using dielectric-barrier discharge plasmas, Plasma Chem. Plasma Proc. 21 (2001) 301-310.

[5] G. Scarduelli, G. Guella, D. Ascenzi, P. Tosi, Synthesis of Liquid Organic Compounds from CH_4 and CO_2 in a Dielectric Barrier Discharge Operating at Atmospheric Pressure, Plasma Process. Polym. 8 (2011) 25–31.

[6] T. Nozaki, A. Ağıral, S. Yuzawa, J.G.E.H. Gardeniers, K. Okazaki, A single step methane conversion into synthetic fuels using microplasma reactor, Chem. Eng. J. 166 (2011) 288–293.

[7] Y. Zhang, Y. Li, Y. Wang, C. Liu, B. Eliasson, Plasma methane conversion in the presence of carbon dioxide using dielectric-barrier discharges, Fuel Process. Technol. 83 (2003) 101–109.

[8] V. Goujard, T. Nozaki, S. Yuzawa, A. Ağıral, K. Okazaki, Plasma-assisted partial oxidation of methane at low temperatures: numerical analysis of gas-phase chemical mechanism, *J*. Phys. D: Appl. Phys. 44 (2011) 274011.

[9] C. De Bie, B. Verheyde, T. Martens, J. van Dijk, S. Paulussen, A. Bogaerts, Fluid Modeling of the Conversion of Methane into Higher Hydrocarbons in an Atmospheric Pressure Dielectric Barrier Discharge, Plasma Process. Polym. 8 (2011)1033–1058.

[10] X. Tu, J.C. Whitehead, Plasma-catalytic dry reforming of methane in an atmospheric dielectric barrier discharge: Understanding the synergistic effect at low temperature, Appl. Catal. B: Environmental 125 (2012) 439-448.

[11] T. C. Manley, The electric characteristics of the ozonator discharge, Transactions of The Electrochemical Society 84(1) (1943) 83-96.

[12] Z. Falkenstein, J. Coogan, Microdischarge behaviour in the silent discharge of nitrogen-oxygen and water-air mixtures, J. Phys. D-Appl. Phys. 30 (1997) 817-825.

[13] R. G. Parr, W. Yang, Density Functional Theory of Atoms and Molecules, Oxford University Press, New York, 1989, Ch. 3.

[14] Y. Zhao, D. G. Truhlar, The M06 suite of density functionals for main group thermochemistry, thermochemical kinetics, noncovalent interactions, excited states, and transition elements: two new functionals and systematic testing of four M06-class functionals and 12 other functionals, Theor. Chem. Acc. 120 (2008) 215-241.

[15] Y. Zhao, D. G. Truhlar, Density functionals with broad applicability in chemistry, Acc. Chem. Res. 41 (2008) 157-167.

[16] Y. Zhao, D. G. Truhlar, How well can new-generation density functionals describe the energetics of bond-dissociation reactions producing radicals?, J. Phys. Chem. A 112 (2008) 1095-1099.

[17] Y. Zhao, D. G. Truhlar, Exploring the Limit of Accuracy of the Global Hybrid Meta Density Functional for Main-Group Thermochemistry, Kinetics, and Noncovalent Interactions, J. Chem. Theory & Comput., 4 (2008) 1849-1868.

[18] E. Woon and T. H. Dunning Jr., Gaussian basis sets for use in correlated molecular calculations. III. The atoms aluminum through argon, J. Chem. Phys. 98 (1993) 1358-1371.

[19] J. A. Pople, P. M. W. Gill, B. G. Johnson, Kohn—Sham density-functional theory within a finite basis set, Chem. Phys. Lett. 199 (1992) 557-560.

[20] H. B. Schlegel, in *Computational Theoretical Organic Chemistry*, edited by I. G. Csizsmadia and R. Daudel (Reidel Publishing Co., Dordrecht, The Netherlands, 1981), p. 129-159.

[21] H. B. Schlegel, An efficient algorithm for calculating ab initio energy gradients using s, p Cartesian Gaussians, J. Chem. Phys. 77 (1982) 3676-3681.

[22] H. B. Schlegel, J. S. Binkley, J. A. Pople, First and second derivatives of two electron integrals over Cartesian Gaussians using Rys polynomials, J. Chem. Phys. 80 (1984) 1976-1981.

[23] H. B. Schlegel, Optimization of equilibrium geometries and transition structures, J. Comput. Chem. 3 (1982) 214-218.

[24] S. Yamanaka, T. Kawakami, K. Nagao, K. Yamaguchi, Effective exchange integrals for open-shell species by density functional methods, Chem. Phys. Lett. 231 (1994) 25-33.

[25] K. Yamaguchi, F. Jensen, A. Dorigo, K. N. Houk, A spin correction procedure for unrestricted Hartree-Fock and Møller-Plesset wavefunctions for singlet diradicals and polyradicals, Chem. Phys. Lett. 149 (1988) 537-542.

[26] Reaction enthalpies and entropies were computed as outlined, for instance, in: Foresman, J. B.; Frisch, Æ. Exploring Chemistry with Electronic Structure Methods, Gaussian, Inc., Pittsburgh, PA (USA), 1996, pages 166-168.

[27] H. Eyring, The Activated Complex in Chemical Reactions, J. Chem. Phys. 3 (1935), 107-115.

[28] A.G. Baboul, H. B. Schlegel, Improved method for calculating projected frequencies along a reaction path, J. Chem. Phys. 107 (1997) 9413-9417.

[29] Gaussian 09, Revision A.1, M. J. Frisch, G. W. Trucks, H. B. Schlegel, G. E. Scuseria, M. A. Robb, J. R. Cheeseman, G. Scalmani, V. Barone, B. Mennucci, G. A. Petersson, H. Nakatsuji, M. Caricato, X. Li, H. P. Hratchian, A. F. Izmaylov, J. Bloino, G. Zheng, J. L. Sonnenberg, M. Hada, M. Ehara, K. Toyota, R. Fukuda, J. Hasegawa, M. Ishida, T. Nakajima, Y. Honda, O. Kitao, H. Nakai, T. Vreven, J. A. Montgomery, Jr., J. E. Peralta, F. Ogliaro, M. Bearpark, J. J. Heyd, E. Brothers, K. N. Kudin, V. N. Staroverov, R. Kobayashi, J. Normand, K. Raghavachari, A. Rendell, J. C. Burant, S. S. Iyengar, J. Tomasi, M. Cossi, N. Rega, J. M. Millam, M. Klene, J. E. Knox, J. B. Cross, V. Bakken, C. Adamo, J. Jaramillo, R. Gomperts, R. E. Stratmann, O. Yazyev, A. J. Austin, R. Cammi, C. Pomelli, J. W. Ochterski, R. L. Martin, K. Morokuma, V. G. Zakrzewski, G. A. Voth, P. Salvador, J. J. Dannenberg, S. Dapprich, A. D. Daniels, Ö. Farkas, J. B. Foresman, J. V. Ortiz, J. Cioslowski, D. J. Fox, Gaussian, Inc., Wallingford CT, 2009.

[30] R. Snoeckx, R. Aerts, X. Tu, A. Bogaerts, Plasma-based dry reforming: a computational study ranging from the nanoseconds to seconds time scale, J. Phys. Chem. 117 (2013) 4957-4970.

[31] J.-G. Wang, C.-J. Liu, Y.-P. Zhang, B. Eliasson, A DFT study of synthesis of acetic acid from methane and carbon dioxide, Chem. Phys. Letters 368 (2003) 313–318.

[32] C L.K. Huynh, A. Violi, Thermal decomposition of methyl butanoate: Ab initio study of a biodiesel fuel surrogate, J. Org. Chem. 73 (2008) 94-101.

[33] C. Anastasi, P.R. Maw, Reaction kinetics in acetyl chemistry over a wide range of temperature, J. Chem. Soc. Faraday Trans. 1, 78 (1982) 2423-2433.

[34] D.L. Baulch, C.J. Cobos, R.A. Cox, P. Frank, G. Hayman, Th. Just, J.A. Kerr, T. Murrells, M.J. Pilling, J. Troe, R.W. Walker, J. Warnatz, Evaluated Kinetic Data for Combustion Modeling, J. Phys. Chem. Ref. Data 23 (1994) 847-1033.

[35] K.W. Watkins, W.W. Thompson, Addition of ethyl radicals to carbon monoxide. Kinetic and thermochemical properties of the propionyl radical, Int. J. Chem. Kinet. 5 (1973) 791-803.

[36] W. Tsang, R.F. Hampson, Chemical Kinetic Data Base for Combustion Chemistry. Part I. Methane and Related Compounds , J. Phys. Chem. Ref. Data 15 (1986) 1087-1279.

[37] W.M.F. Fabian, R Janoschek, Thermochemical properties of the hydroxy-formyl radical, HO-(CO)-C$^{\bullet}$, and the formyloxy radical, HC(O)O$^{\bullet}$, and their role in them reaction (OH)-O$^{\bullet}$+CO → H$^{\bullet}$+CO_2. Computational G3MP2B3 and CCSD(T)-CBS studies, Journal of Molecular Structure (THEOCHEM) 713 (2005) 227–234.

[38] D. Feller, D.A. Dixon, J.S. Francisco, Coupled cluster theory determination of the heats of formation of combustion-related compounds: CO, HCO, CO_2, HCO_2, HOCO, HC(O)OH, and HC(O)OOH, J. Phys. Chem. A 107 (2003) 1604-1617.

[39] T.V. Duncan, C.E. Miller, The HCO_2 potential energy surface: Stationary point energetics and the HOCO heat of formation, J. Chem. Phys. 113 (2000) 5138-5140.

[40] C.F. Melius, BAC-MP4 Method, Heats of Formation and Free Energies, Sandia National Laboratories, Livermore CA, August 28, 1997.

[41] J.P. Senosiain, S.J. Klippenstein, J.A. Miller, A complete statistical analysis of the reaction between OH and CO , Proc. Combust. Inst. 30 (2005) 945–953.

[42] H.-G. Yu, J.T. Muckerman, T.J. Sears, A theoretical study of the potential energy surface for the reaction OH+CO → H+CO_2, Chem. Phys. Lett. 349 (2001) 547–554.

[43] S. De Benedictis, G. Dilecce, Low Temperature Plasma Technology: Methods and Applications (2013), Paul K. Chu, XinPei Lu Ed., chapter 9, 261-284 CRC Press.